iScience, Volume *24*

Supplemental information

Renal subcapsular delivery of PGE_2 promotes kidney repair by activating endogenous $Sox9^+$ stem cells

Shang Chen, Haoyan Huang, Yue Liu, Chen Wang, Xiaoniao Chen, Yuqiao Chang, Yuhao Li, Zhikun Guo, Zhibo Han, Zhong-Chao Han, Qiang Zhao, Xiang-Mei Chen, and Zongjin Li

iScience, Volume ■ ■

Supplemental information

Renal subcapsular delivery of PGE_2 promotes kidney repair by activating endogenous $Sox9^+$ stem cells

Shang Chen, Haoyan Huang, Yue Liu, Chen Wang, Xiaoniao Chen, Yuqiao Chang, Yuhao Li, Zhikun Guo, Zhibo Han, Zhong-Chao Han, Qiang Zhao, Xiang-Mei Chen, and Zongjin Li

SUPPLEMENTAL INFORMATION

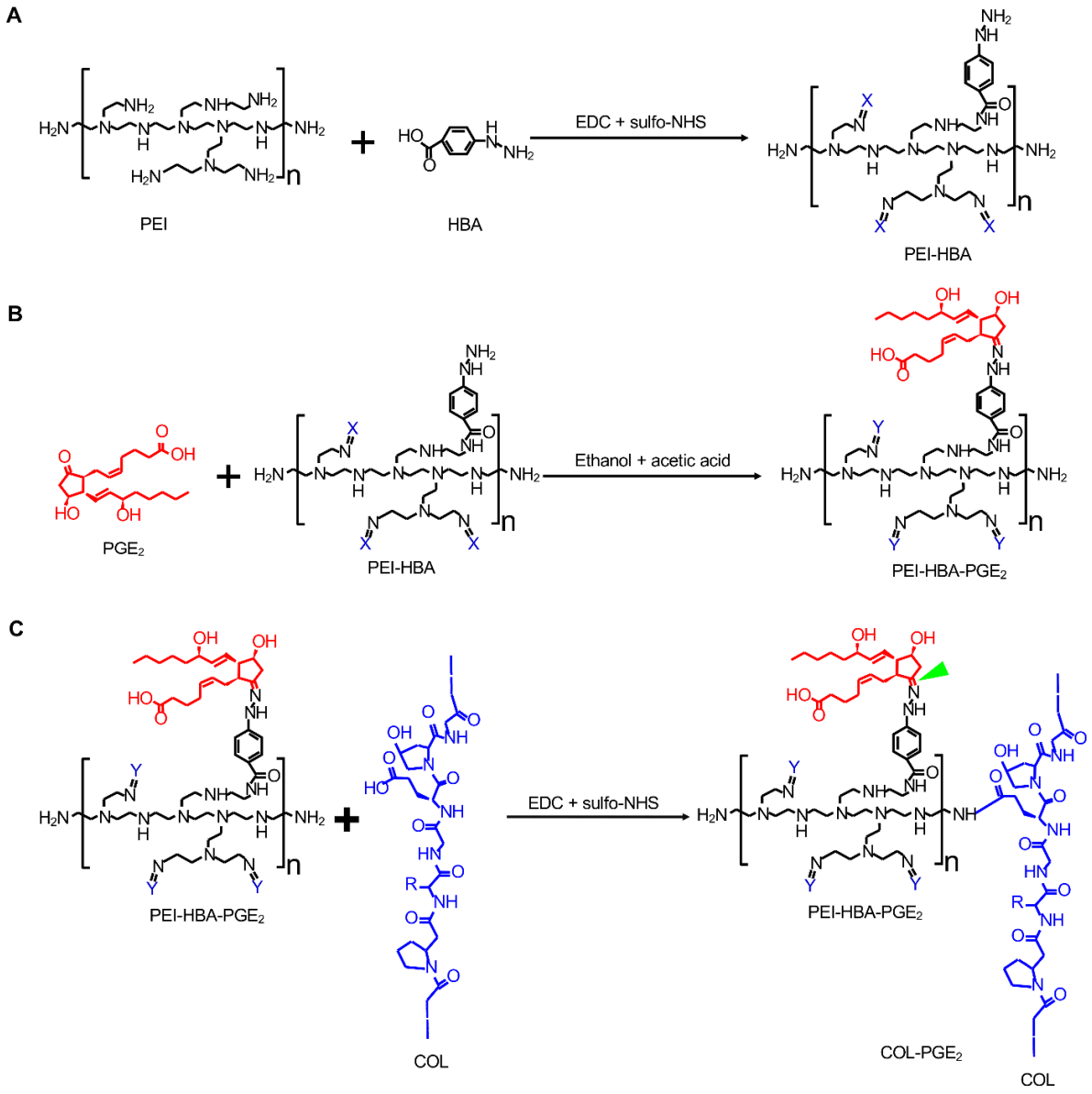

Figure S1. A schematic depicting the method of synthesis of the COL-PGE$_2$ matrix. (**A**) The PEI-HBA conjugates were synthesized by the dehydration condensation reaction between the amine group on PEI and the carboxylic group on HBA. (**B**) The ketone group on PGE$_2$ was reacted with the hydrazine group on PEI-HBA to synthesize the PEI-HBA-PGE$_2$ conjugates through a dehydration reaction. (**C**) The PEI-HBA-PGE$_2$ conjugates and collagen were further crosslinked by using dehydration condensation. Mechanism of PGE$_2$ release: The breakage sites of PGE$_2$ covalently attached (red) to branched PEI-HBA (black) and collagen (blue) are indicated by green arrows. X= hydrogen or HBA; Y = hydrogen, HBA or HBA-PGE$_2$. Abbreviations: HBA, 4-hydrazinobenzoic acid; PEI, polyethyleneimine.

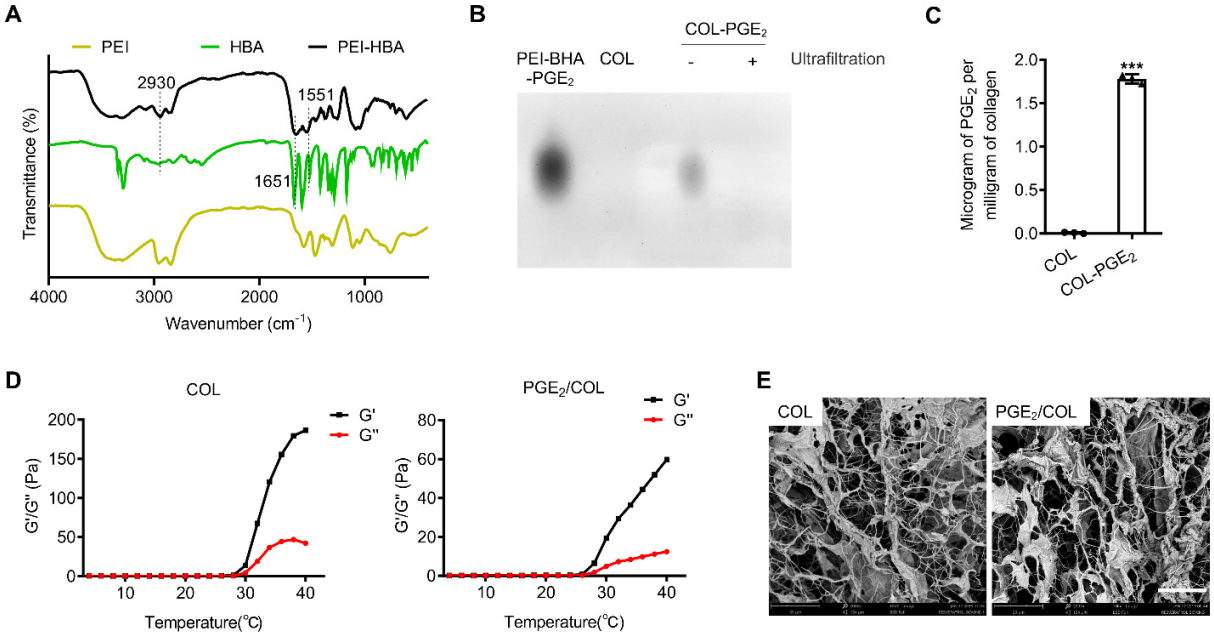

Figure S2. Characterization of collagen and the PGE_2/COL matrix. (**A**) FT-IR analysis shows the characteristic peaks of PEI, HBA, and PEI-HBA. (**B**) Tris-borate-EDTA–PAGE was used to detect free PEI-HBA-PGE_2. (**C**) Quantification of PGE_2 in collagen before and after crosslinking as determined using ELISA. Results are normalized to collagen concentration and expressed as the content of PGE_2 per milligram of collagen. The two-tailed *t* test was used for statistical analysis. Data are expressed as mean ± SD; $^{***}P <$ 0.001 versus COL. The experiments were carried out in triplicate. (**D**) Evaluation of the rheologic profile of collagen (left) and the PGE_2/COL matrix (right) during temperature changes. (**E**) Scanning electron micrograph image that reveals the morphologic structure of lyophilized collagen (left) and the PGE_2/COL matrix (right). Scale bars, 30 μm.

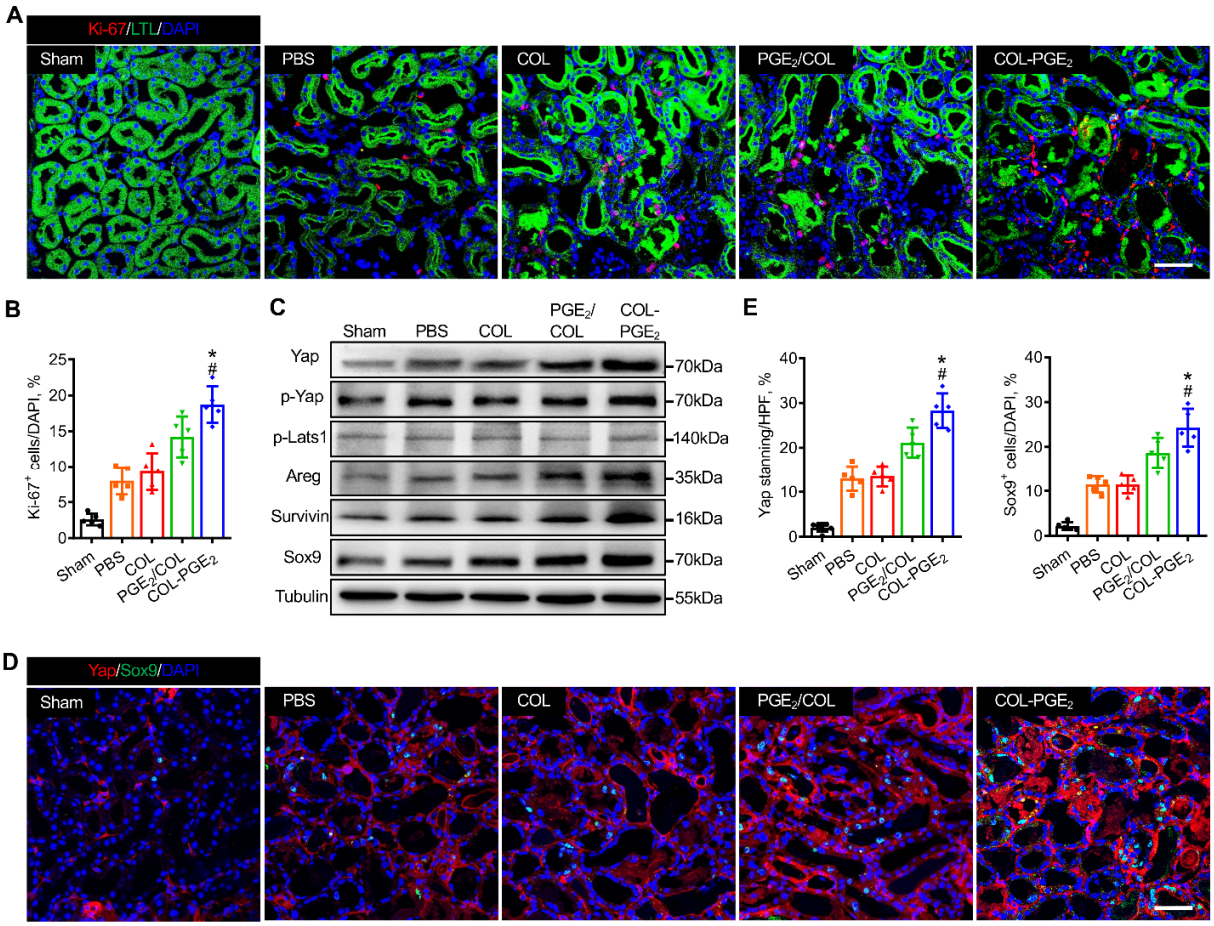

Figure S3. COL-PGE2 promoted the proliferation of proximal tubular epithelial cells and the activation of Sox9 through Yap mediation. (**A**) Representative images show Ki-67 immunostaining (red) detected in proximal tubular epithelial cells (LTL, green) on day 3 after AKI. (**B**) Quantification of Ki-67^{+} staining in (**A**). (**C**) Immunoblot analysis of the YAP, p-YAP, p-Lats1, Arge, Survivin, and Sox9 protein in the kidney on day 3 of PBS, COL, PGE_2/COL and COL-PGE2. (**D**) Immunostaining analysis of YAP (red) and Sox9 (green) on day 3 after AKI. (**E**) Quantification of YAP^{+} (left) and Sox9^{+} (right) staining. HPF, high-power field. Scale bars, 50 μm. One-way repeated measures ANOVA with Tukey post hoc tests (B and E) was used for statistical analysis. Data are expressed as mean ± SD; n=5, $^{*}P < 0.05$ versus COL; $^{\#}P < 0.05$, versus PGE_2/COL.

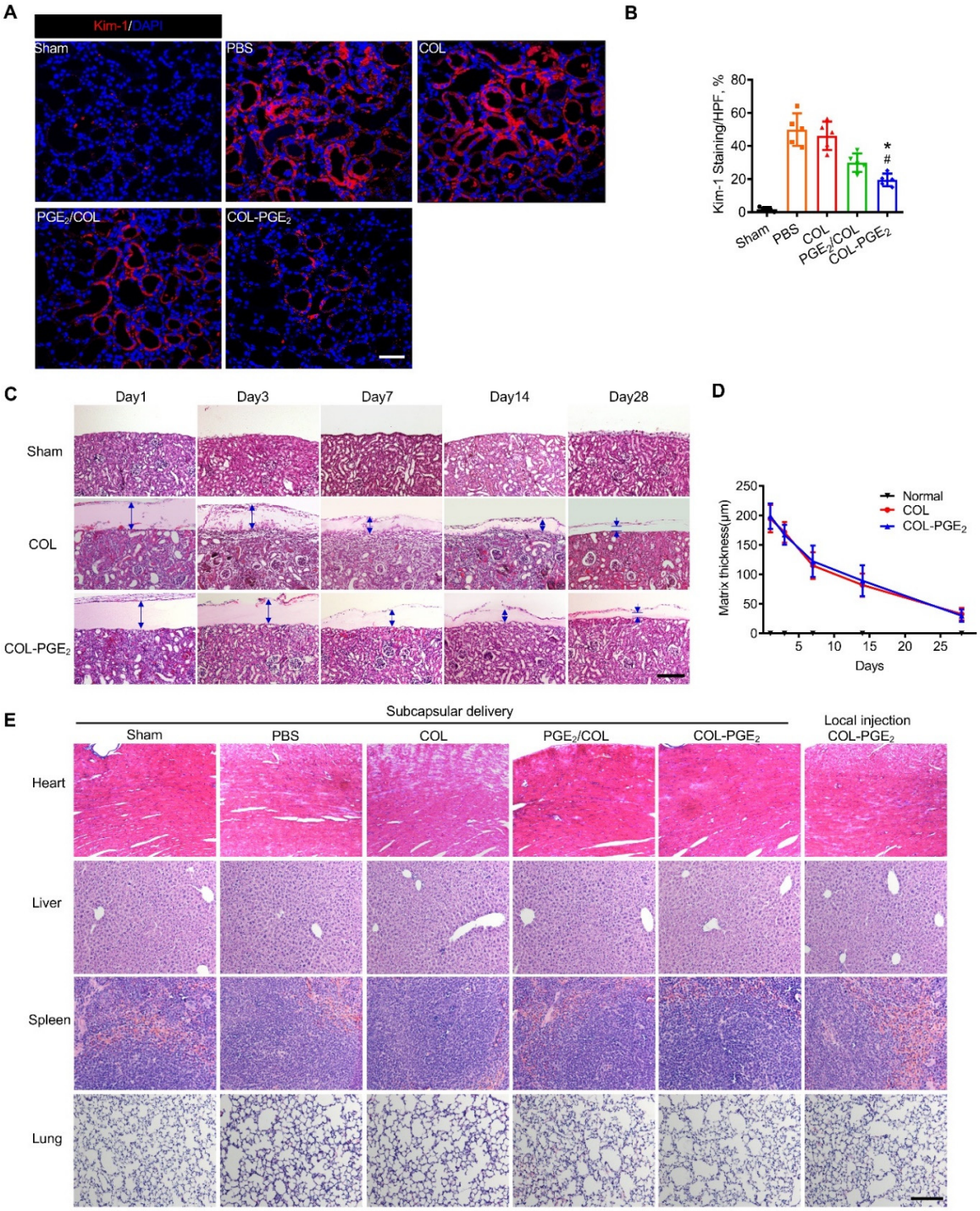

Figure S4. The COL-PGE2 matrix attenuates kidney injury without organ toxicity. (**A**) Histological analysis of kidney injury by anti-Kim-1 immunostaining (red) on day 3 post AKI. Scale bars, 50 μm. (**B**) Quantification of Kim-1$^+$ staining. (**C**) Analysis of the matrix degradation profile by measuring the thickness of the matrix under the kidney capsules on day 1, 3, 7, 14, 28 post AKI. Scale bars, 200 μm. (**D**) Quantification of the thickness of the matrix. (**E**) H&E staining did not show histological changes in the heart, liver, spleen and lung. One-way repeated measures ANOVA with a Tukey post hoc test (**B**) and Two-way multivariate analysis of variance (two-way MANOVA) with Tukey post hoc test (D) were used for statistical analysis. Data are expressed as mean ± SD; n=5, $^*P < 0.05$ versus COL; $^{\#}P < 0.05$, versus PGE_2/COL.

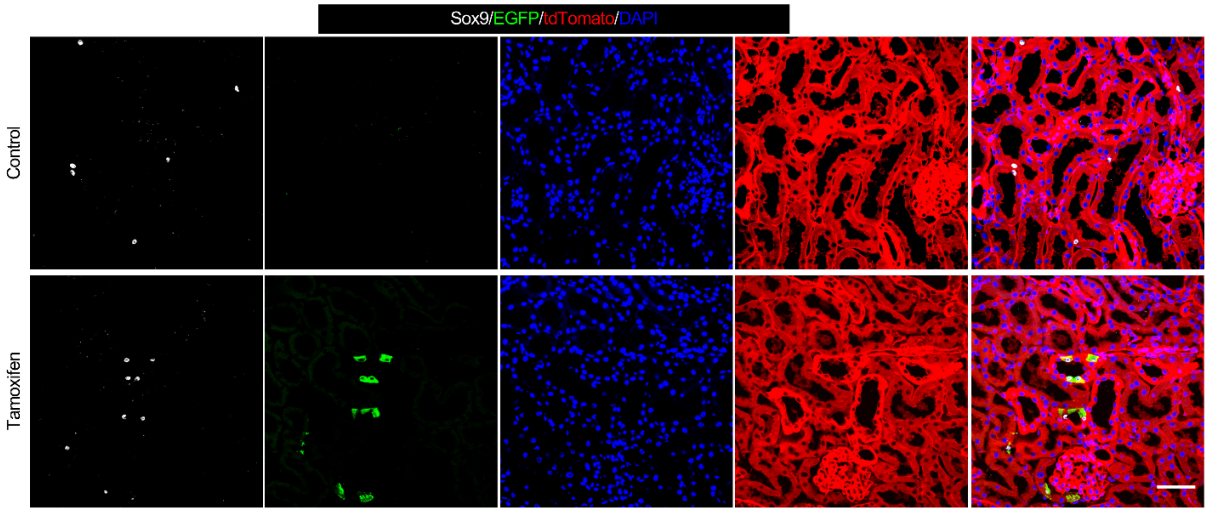

Figure S5. Validation of the Sox9-Cre^{ERT2}; R26^{mTmG} mouse genetic model
To verify the mouse genetic model, tamoxifen (corn oil was used as a control) was injected three times in succession before AKI, and Sox9^{+} cells and EGFP fluorescence colocalization in the kidney were detected by anti-Sox9 immunostaining.

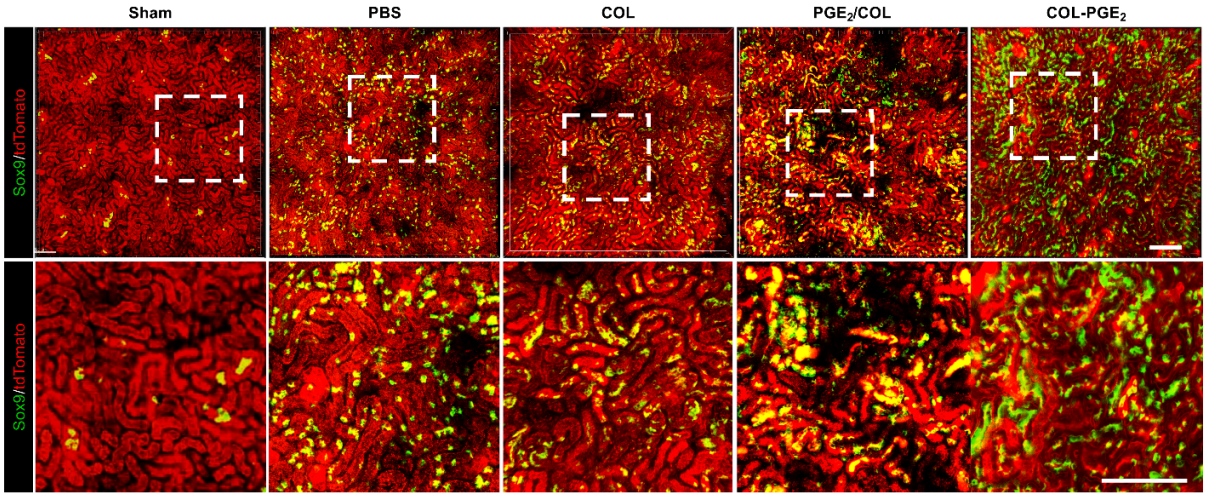

Figure S6. Two-photon living imaging of Sox9$^+$ cell expansion following PGE_2 treatment. Representative images of two-photon intravital tracing showed that Sox9$^+$ cell-derived cells were abundantly expanded by the administration of COL-PGE_2 matrix on day 7 after AKI. Scale bar, 200 μm. See also Video S1-4.

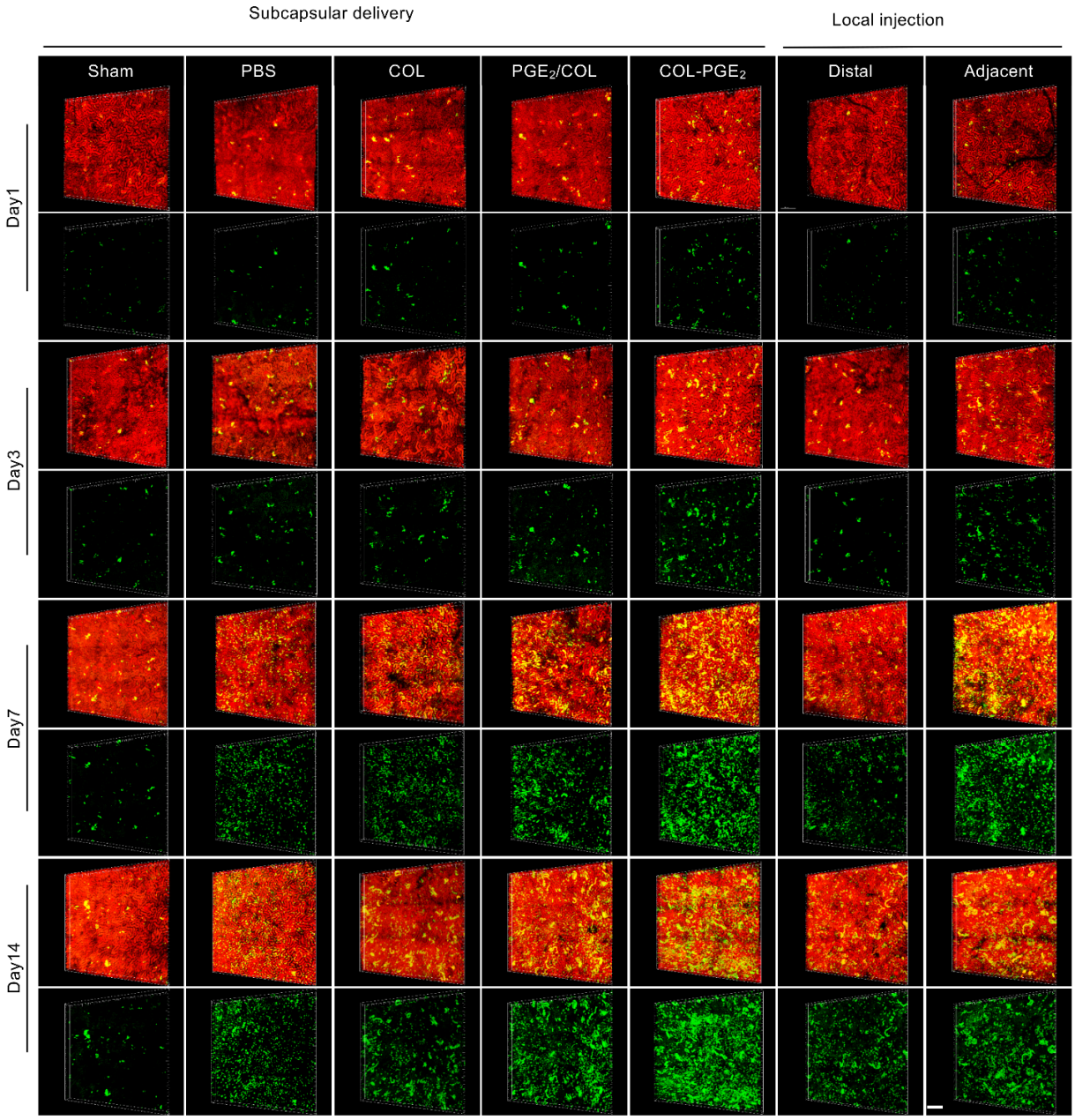

Figure S7. The COL-PGE2 matrix promoted the formation of functional renal tubules in descendants of Sox9^{+} cells. Representative images of two-photon intravital microscopy showed Sox9+ derived cells with the administration of PBS, COL, PGE2/COL and COL-PGE2 matrix at different time points after AKI. Scale bar, 200 μm.

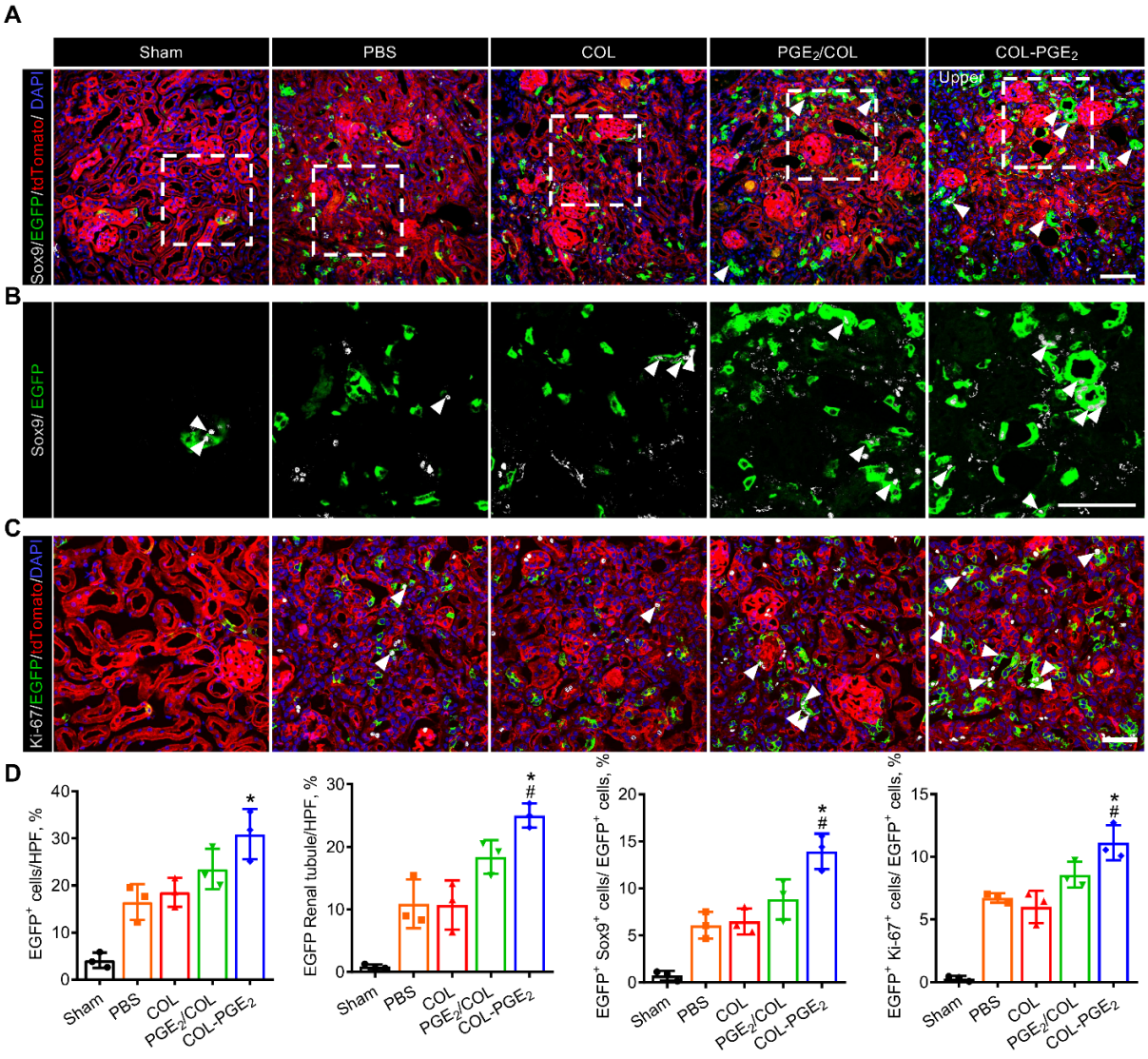

Figure S8. The COL-PGE2 matrix results in increased activation of Sox9 expression and Sox9$^+$ cell proliferation (**A**) Confocal images and (**B**) local zoomed-in images for colocalization analysis of anti-Sox9 immunostaining (gray) and Sox9-Cre^{ERT2}-activated EGFP fluorescence in kidneys with the administration of the PBS, COL, PGE_2/COL and COL-PGE_2 matrix on day 14 post AKI. White arrowheads highlight Sox9$^-$ EGFP-labeled cells, and white arrowheads highlight Sox9$^+$/EGFP-colabeled cells. Scale bar, 50 μm. (**C**) Confocal images for the colocalization analysis of anti-Ki-67 immunostaining (gray) and Sox9-Cre^{ERT2}-activated EGFP fluorescence in kidneys with the administration of PBS, COL, PGE_2/COL and COL-PGE_2 matrix on day 14 after injury. White arrowheads highlight Ki-67$^+$/EGFP colabeled cells. Scale bar, 50 μm. (**D**) Quantification of EGFP+ cells, EGFP renal tubules, Sox9$^+$/EGFP colabeled cells and Ki-67$^+$/EGFP colabeled cells in the kidneys of mice on day 14 after delivery of the COL-PGE_2 matrix post AKI. One-way repeated measures ANOVA with a Tukey post hoc tests (D) were used for statistical analysis. Data are expressed as mean ± SD; n=3, $^*P < 0.05$ versus COL; $^{\#}P < 0.05$, versus PGE_2/COL.

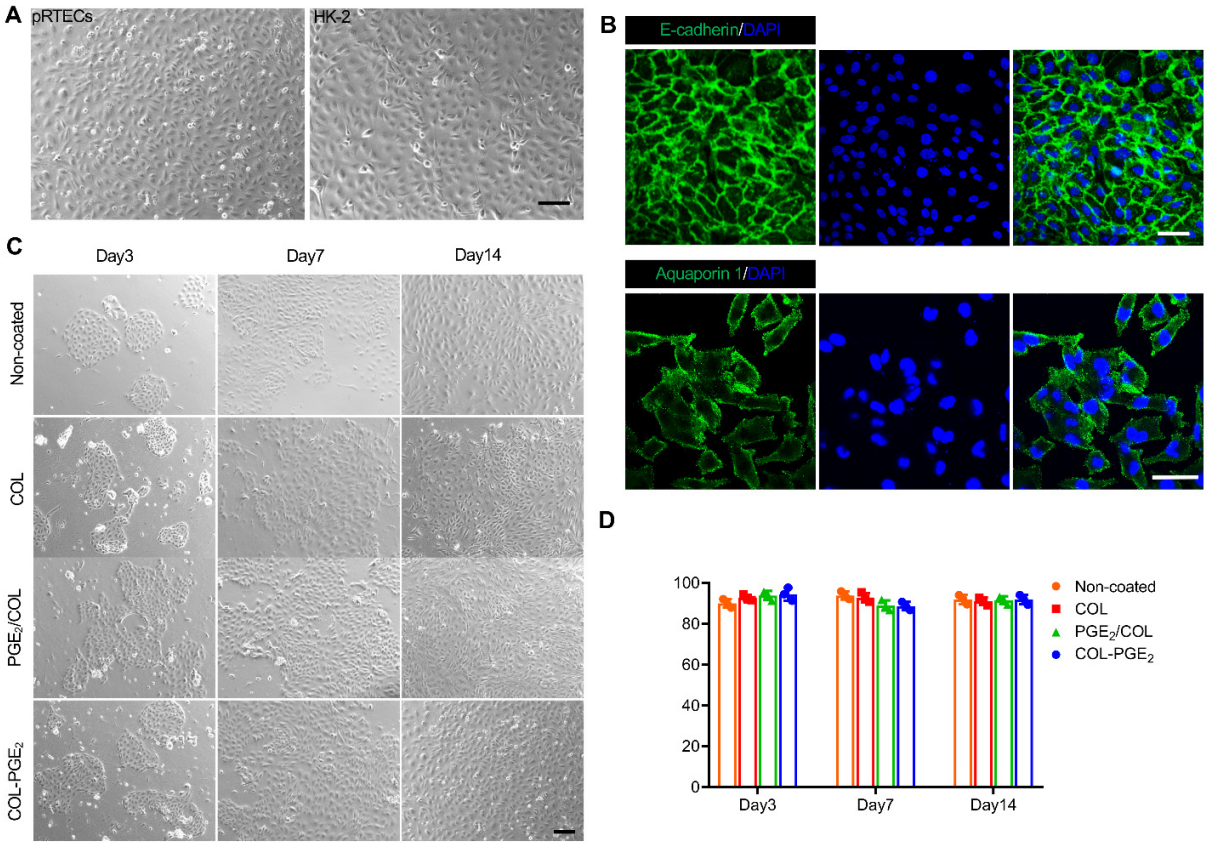

Figure S9. Renal tubular epithelial cell morphology and matrix biocompatibility. (**A**) Comparison of the morphology between isolated primary renal tubular epithelial cells (pRTEC) and HK-2 human renal proximal tubule cells. Scale bar, 100 μm. (**B**) Immunofluorescence staining with antibodies against E-cadherin (top) and Aquaporin-1 (bottom) shows the isolated pRTECs. Scale bar, 50 μm. (**C**) The morphology and colony formation capacity of pRTEC cultured on noncoated or COL, PGE_2/COL or COL-PGE_2 matrix for 3, 7, and 14 days. Scale bar, 100 μm. (**D**) Quantification of cell viability by trypan blue staining and calculation of the percentage of live cells cultured on noncoated or COL, PGE_2/COL or COL-PGE_2 matrix-coated plates for 3, 7, and 14 days. Two-way MANOVA with Tukey post hoc test was used for statistical analysis. Data are expressed as mean ± SD; All data are representative of three independent experiments and are shown as mean ± SD.

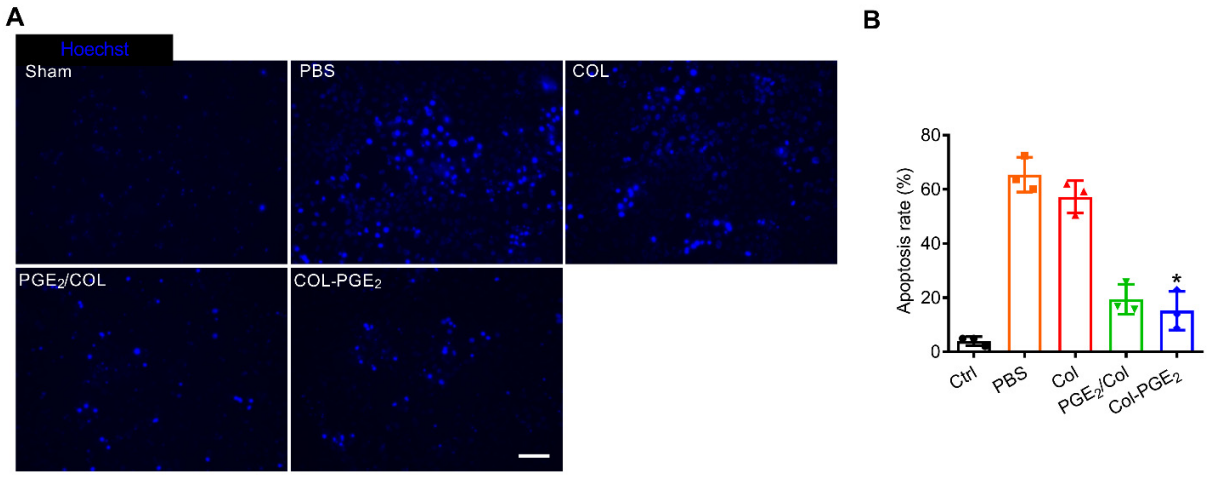

Figure S10. COL-PGE_2 matrix exerts an anti-apoptosis effect *in vitro*. (**A**) Hoechst 33342 staining showed the survival of pRTECs cultured on noncoated, PBS, COL, PGE_2/COL or COL-PGE_2-coated plates upon exposure to 150 μM H_2O_2 for 6 h. Scale bar, 100 μm. (**B**) Quantification of the apoptosis index of pRTECs under H_2O_2-induced stress. One-way repeated measures ANOVA with a Tukey post hoc test (B) was used for statistical analysis. Data are expressed as mean ± SD, n=3, $^*P < 0.05$ versus COL.